C. R. Chimie 17 (2014) 91–102

Contents lists available at SciVerse ScienceDirect

Comptes Rendus Chimie

www.sciencedirect.com

Full paper/Mémoire

Polyaniline/$CoFe_2O_4$ nanocomposite inhibits the growth of *Candida albicans* 077 by ROS production

Javed Alam Khan [a,1], Mohd Qasim [b,1], Braj Raj Singh [a,*], Wasi Khan [a], Dibakar Das [b], Alim H. Naqvi [a]

[a] *Centre of Excellence in Materials Science (Nanomaterials), Department of Applied Physics, Z.H. College of Engineering and Technology, Aligarh Muslim University, Aligarh 202002, UP, India*
[b] *School of Engineering Sciences and Technology (SEST), University of Hyderabad, Hyderabad 500 046, AP, India*

ARTICLE INFO

Article history:
Received 11 April 2013
Accepted after revision 19 August 2013
Available online 26 September 2013

Keywords:
Polyaniline/$CoFe_2O_4$
Nanocomposite
Candida albicans
Anticandidal
ROS

ABSTRACT

In recent years, polyaniline/$CoFe_2O_4$ nanocomposites have gained attention because of their wide utilization in optoelectronics and biomedical studies. However, very limited research has been carried out on the anticandidal activity of polyaniline/$CoFe_2O_4$ nanocomposite against *Candida* spp. Thus, the study was designed to investigate the anticandidal potential of PANI/$CoFe_2O_4$ nanocomposite against *Candida albicans* 077. PANI/$CoFe_2O_4$ nanocomposite (denoted as "cfPNCs") was synthesized by polymerization of aniline in the presence of $CoFe_2O_4$ nanoparticles. The structural and thermal properties of the synthesized PANI/$CoFe_2O_4$ nanocomposite were investigated. It was noteworthy that PANI/$CoFe_2O_4$ nanocomposite showed promising anticandidal activity in a dose-dependent manner. Results also showed that the protection of histidine (a ROS quencher) against ROS clearly suggested the implication of ROS in anticandidal activity of PANI/$CoFe_2O_4$ nanocomposite. It is encouraging to conclude that PANI/$CoFe_2O_4$ nanocomposite bears the potential of their applications in biomedicine, especially nanotherapy for diseases caused by *C. albicans*.

1. Introduction

Polyaniline (PANI) is a conducting polymer that has received immense attention in recent years owing to its physical, chemical and biological properties [1]. Therefore, the PANI-containing polymeric nanocomposites (PNCs) are widely being used for the fabrication and development of bioelectronics, optoelectronics, and sensor-based devices [2,3]. Among them, particularly, the PNCs of metal oxides such as cobalt iron oxide ($CoFe_2O_4$) nanoparticles (NPs) have been studied extensively to understand their unique physicochemical properties, not only for scientific research, but also for technological applications [4]. $CoFe_2O_4$ belongs to the family of spinel-type ferrites and is one of the most important ferrites, with high coercivity, moderate magnetization, high magnetocrystalline anisotropy, chemical stability, and mechanical hardness [5]. These $CoFe_2O_4$-based PNCs frequently exhibit unexpected hybrid properties derived from both components and have great potential applications in the areas of electronics, photonics, catalysis, etc. [6].

Magnetic NPs of iron oxides and their hybrid forms represent the most suitable candidates for the preparation of magnetic nanocomposites owing to their application-convenient magnetic (e.g., superparamagnetism) and biochemical (e.g., non-toxicity, biocompatibility, biodegradability) properties and low price. These oxides that can

* Corresponding author.
E-mail address: brajviro@gmail.com (B.R. Singh).
[1] These authors contributed equally.

1631-0748/$ – see front matter
http://dx.doi.org/10.1016/j.crci.2013.08.006

play the role of nano-antimicrobial agents are believed to be non-toxic, and some of them even contain mineral elements essential to the human body [7]. Moreover, biomedical applications of polyaniline/$CoFe_2O_4$ nanocomposite have also been reported in recent years owing to its suitable magnetic behaviour at room temperature for MRI contrast enhancement and hyperthermia treatments [8]. Although conventional antibacterial agents have several disadvantages, i.e., toxicity to the microbiota and sensitivity towards the temperatures and pressures [9], therefore, the interest in metal-oxide-based nano-antimicrobial agents are rising over the years [10,11]. These metal-oxide-based nano-antimicrobial agents exhibited strong antimicrobial activity at low concentrations, with high stability in extreme conditions [12,13]. The suggested mechanism for the antimicrobial activity of metal-oxide-based NPs is based mainly on the production of reactive oxygen species (ROS) from the catalysis of water [14]. Although many controversies have been raised on the mechanistic aspects of the antimicrobial activity of the metal oxide NPs, there is copious evidence that metal-oxide-based NPs increase oxidative stress through the generation of reactive oxygen species (ROS) that include predominantly hydroxyl radicals ($^{\bullet}OH$) and singlet oxygen ($^1O_2$). These ROS mainly contribute to the antimicrobial activity of metal-oxide-based NPs [14,15]. Other antimicrobial mechanisms involving metal-oxide-based NPs, like cytoplasmic membrane disruption and electrostatic binding of metal oxide NPs to the cell surface of the microbial pathogen, have been reported [16–18]. However, recently the production of ROS governed by the electronic band gap property of metal-oxide-based NPs has been considered as triggering the actual mechanism [14]. The energy band gap property of metal-oxide-based NPs are influenced by various physical and chemical parameters [19]. Therefore, a fundamental understanding of the energy band gap property of metal-oxide-based NPs becomes crucial to the tailoring of novel nano-antimicrobial agents in an economic way.

Recent preliminary studies on $CoFe_2O_4$ NPs have demonstrated that they may be appropriate antimicrobial agents to control and manage human microbial pathogens [20,21]. Ferrite NPs exhibit an intrinsic peroxidase-like activity by generating ROS via the Fenton reaction [22]. $CoFe_2O_4$ NPs interacts with the microbial cell surface and elevates the oxidative stress that disrupts the integrity of the cell wall/membrane and damage the biological macromolecules [23]. Although NPs coated with polymers exhibited stronger antimicrobial activity in comparison to the bare [24], extensive work has been done in recent years to develop promising nanocomposite antibacterial agents based on synthetic materials or biopolymers. These polymers possess an intrinsic antibacterial activity through (*i*) coating or adsorption of an antibacterial agent onto the polymer surface; (*ii*) grafting/fabrication of an antibacterial agent in the polymer via ionic or covalent bonding, or (*iii*) direct incorporation of an antibacterial agent into the polymer during in situ synthesis [25,26]. Among them, conducting polymer polyaniline (PANI) has inherently a broad spectrum of antibacterial and antifungal properties. Thus, the PANI has been the subject of considerable attention due to its potential in biomedical applications [27,28]. These findings motivated us to use PANI/$CoFe_2O_4$ composite as an anticandidal agent.

Over the past years, researches have been carried out on the assessment of the antimicrobial activity of NPs and nanomaterials. However, research focused on the antimicrobial properties of NPs and nanomaterials were confined to the prokaryotic pathogens in comparison to the eukaryotic pathogens. Therefore, in this study, we have chosen *Candida albicans*, an eukaryotic human pathogen, for assessment of the anticandidal properties of PANI/$CoFe_2O_4$ nanocomposite. *C. albicans* is amongst the most common fungal causative agent in superficial and deep-seated candidiasis, depending on the patient's immune system status [29]. The brutality of antifungal drugs in pharmacotherapy has led to the development of widespread multi-drug resistance (MDR) in *C. albicans* [30]. The failure of antifungal drugs to control infection makes it crucial to find alternatives to currently available drugs. Unfortunately, most of these antifungal drugs chemical in nature and bulk form that are being investigated are too reactive and are unsuitable for the treatment of *C. albicans* infections in humans [31]. With the continuous development of MDR in *C. albicans*, the search for new medical treatments beyond conventional antifungal drugs has become a key aim of public health research [32]. Possible innovative strategies encompass the inhibition of *C. albicans* growth with the use of NPs and nanomaterials [33]. There is thus a need for the identification of a novel class of PNCs that can be able to inhibit efficiently *C. albicans* growth. Identification of such metal-oxide-based or hybrid nano-antimicrobial agents could present us with new opportunities for the development of novel non-antibiotic drugs for treating *C. albicans* diseases [30,32,33]. The anticandidal activity of PANI/$CoFe_2O_4$ against *C. albicans* has not been studied yet. Therefore, in this study, we have synthesized a stable and surface-protected PANI/$CoFe_2O_4$ nanocomposite (denoted as "cfPNCs") using a conducting polymer and investigated its anticandidal activity against *C. albicans* 077.

2. Materials and methods

2.1. Materials

All reagents were of analytical grade. Cobalt nitrate, iron nitrate, ammonium peroxydisulfate, citric acid, *N*-methyl-2-pyrrolidone (NMP) and hydrochloric acid were purchased from SRL, India. The nutrient media, Sabouraud's dextrose (SD) broth and agar for the *C. albicans* 077 were obtained from the HiMedia Laboratories, Mumbai, India. Histidine and 2,7-dichlorofluorescin diacetate (DCFH-DA) was purchased from Sigma-Aldrich (St. Louis, Missouri, USA). All other chemicals used were of the highest purity available from commercial sources.

2.2. Nanocomposite materials synthesis

2.2.1. $CoFe_2O_4$ NPs synthesis

$CoFe_2O_4$ NPs were synthesized by the gel-combustion citrate–nitrate method reported previously [34]. The salts

of $Co(NO_3)_3{\cdot}9H_2O$ and Fe $(NO_3)_3{\cdot}9H_2O$ (1:1 molar ratio) were dissolved completely in 100 mL of Milli Q water. In this salt mixture, an equal amount of citric acid (1:1 citric acid/nitrate molar ratio) was added, and the suspension was continuously stirred at a constant temperature at about 90 °C. The pH of the suspension was maintained at ~7.4 to stabilize the nitrate–citrate solution until a high-viscosity wet sol gel was formed. The sol gel was subjected to a high temperature of ~300 °C in an aerobic atmosphere for combustion. The combustion product was a brown, puffy, porous dry gel; calcination of the powder was carried out at 550 °C for 3 h.

2.2.2. PANI/$CoFe_2O_4$ nanocomposite (cfPNCs) synthesis

The cfPNCs was prepared via *in situ* polymerization of aniline in an aqueous solution [35] containing $CoFe_2O_4$ NPs as synthesized (see 2.2.1). Initially, 0.2 M of aniline was dissolved in 1 M HCl and 0.25 g (w/v) of an ultra-sonicated $CoFe_2O_4$ NPs aqueous solution was added. The solution was vigorously stirred to keep $CoFe_2O_4$ NPs suspended. In this solution, 0.625 M $(NH_4)_2S_2O_8$ was added dropwise to the suspension mixture under constant stirring and refrigerated conditions (~4 °C) for ~8 h. The color of the synthesized cfPNCs changed into dark green after polymerization. The resultant cfPNCs was harvested by centrifugation at 5000 rpm for 10 min. The slurry of the cfPNCs thoroughly was washed with 0.1 M HCl, then with MQ water. The final cfPNCs product was dried under vacuum at 60 °C for 24 h, and grounded into powder form. To see the effect of PANI (aniline; 0.1 M, 0.2 M, 0.3 M, 0.4 M, and 0.5 M) on the anticandidal activity, different samples of the cfPNCs were also synthesized.

2.3. PANI/$CoFe_2O_4$ nanocomposite (cfPNCs) characterizations

The synthesis of cfPNCs in solution was monitored by measuring the absorbance (A) using UV-vis spectrophotometer (PerkinElmer Life and Analytical Sciences, CT, USA) in the wavelength range of A_{200} to $A_{800\ nm}$. The $CoFe_2O_4$ NPs and cfPNCs dispersed in NMP were stored at 4 °C for 120 days and the $A_{275\ nm}$ absorbance was measured regularly to ascertain their stability. The vacuum-dried cfPNCs powder was stored in amber color vials at room temperature under dry and dark conditions until used for further characterization. The X-ray diffraction (XRD) patterns of powdered samples were recorded on a MiniFlex™ II benchtop XRD system (Rigaku Corporation, Tokyo, Japan) operating at 40 kV and at a current of 30 mA with Cu Kα radiation (λ = 1.54 Å). The diffracted intensities were recorded from 20° to 80° 2θ angles. The crystalline size (D) [1] of the cfPNCs NPs in the composite was calculated following the Debye–Scherrer formula:

$$D = 0.9\lambda/\beta\cos\theta$$

where λ is the X-ray wavelength, β is the broadening of the diffraction line measured at half of its maximum intensity in radians, and θ is the Bragg diffraction angle. The crystalline size of the cfPNCs was determined by employing the full-width-at-half-maximum (FWHM) value of the (311) XRD peak. For morphological analysis, scanning electron microscopy (SEM) was carried out using the fine powder of the synthesized cfPNCs on a carbon tape in a JSM 6510LV scanning electron microscope (Jeol, Tokyo, Japan) at an accelerating voltage of 20 kV. The elemental analysis was performed using the Oxford Instruments INCAx-sight energy dispersive X-ray (EDAX) spectrometer equipped with SEM. For transmission electron microscopy (TEM) analysis, a drop of aqueous cfPNCs was placed on the carbon-coated copper grid and air dried under dark. The prepared grid was analysed with a Jeol 100/120 kV TEM (JEOL, Tokyo, Japan) with an accelerating voltage of ~150 kV. The electron micrographs and EDAX were obtained and converted into an enhanced metafile format. For FTIR spectroscopic measurements, the cfPNCs powder was mixed with spectroscopic-grade potassium bromide (KBr) at a ratio of 1:100 and spectra were recorded in the 400–4000 cm^{-1} wavenumber range with a PerkinElmer FTIR Spectrum BX (PerkinElmer Life and Analytical Sciences, CT, USA) in the diffuse reflectance mode at a resolution of 4 cm^{-1} in KBr pellets. The thermal stability of the cfPNCs was investigated by thermogravimetric analysis (TGA) (Sieco SII, SSC5100, Instrument) at a heating rate of 10 °C/min under nitrogen atmosphere.

2.4. PANI/$CoFe_2O_4$ nanocomposite (cfPNCs) anticandidal activity

2.4.1. Growth conditions

Clinical isolate *C. albicans* 077 was obtained from the Department of Microbiology, JN Medical College, Aligarh, U.P., India. The stock culture was maintained on slants of SD agar at 4 °C. The primary culture of the *C. albicans* 077 was prepared from the stock slant into the SD broth medium and incubated for 48 h (stationary phase, 10^8 cfu/mL) at 37 °C. The primary culture (~1 mL) was re-inoculated into the 50-mL fresh SD broth and grown for ~12 h up to mid-log phase (~10^5 cfu/mL) at 37 °C. All experiments were performed from the mid-log phase (~10^5 cfu/mL) freshly grown *C. albicans* 077 culture in triplicates.

2.4.2. Anticandidal activity

2.4.2.1. Agar disc diffusion assay. To assess the zone of inhibition of *C. albicans* 077 grown by cfPNCs, an agar disc diffusion assay was performed. Briefly, 5 mL of mid-log phase grown culture of *C. albicans* 077 was centrifuged at 4000 rpm for 5 min at 4 °C. Then the pellet was washed with 1 × PBS and resuspended in 500 μL of a normal saline solution (NSS). Hundred μL of the suspended cells were spread uniformly on SD agar plates and the plates were incubated at 37 °C for 30 min. The seeded petri plates were used for the loading of the various concentrations of cfPNCs (0, 5, 10, and 15 μg/mL) onto filter paper discs. To see the effect of PANI (aniline; 0.1 M, 0.2 M, 0.3 M, 0.4 M, and 0.5 M) on the anticandidal activity, 5 μg/mL of the synthesized cfPNCs were loaded onto the filter paper discs mounted on *C. albicans* 077-seeded petri plates. The Petri plates were incubated at 37 °C for 40 h, then the zone of inhibition was determined by measuring the diameter of *C. albicans* 077 cell clearance.

2.4.2.2. In vitro killing assay. To determine the *in vitro* killing activity of the cfPNCs, the *C. albicans* 077 cell suspension was obtained similarly as described for the agar disc diffusion assay (Section 2.4.2.1). The suspended cells (~100 μL) were dispersed into the 96-well microtiter plate in triplicates. To this, various concentrations of cfPNCs (0, 5, 10, and 15 μg/mL) diluted in 100 μL of a sterile SD broth medium were added and incubated at 37 °C for 2 h. The whole suspension of the plate wells was spread on the SD agar plate and incubated at 37 °C for 40 h. Anticandidal activity was detected by dose-dependent reduction in a number of colony forming units (cfu) in terms of absorbance data.

2.4.2.3. Growth kinetics assay. To see the effect of the cfPNCs on the growth kinetics of *C. albicans*, 50 mL of SD broth in individual flasks were inoculated with 100 μL of the NSS suspended cells of *Candida* cells. The different concentrations of cfPNCs (0, 5, 10, and 15 μg/mL) to be tested were poured in the individual flasks. The flasks were incubated at 37 °C for 40 h and the time-dependent growth kinetics were recorded turbidometrically at $A_{595\ nm}$. The experiment was performed in triplicates and the turbidity background induced by cfPNCs was subtracted from the final reading.

2.5. Intracellular measurement of ROS generation

The production of intracellular reactive oxygen species (ROS) was measured using 2,7-dichlorofluorescin diacetate (DCFH-DA) [36]. The DCFH-DA passively enters the cell, where it reacts with ROS to form the highly fluorescent compound dichlorofluorescein (DCF). Briefly, a DCFH-DA (10 mM) stock solution in methanol (HPLC grade) was diluted in the culture medium to yield a working solution (100 μM). At the end of exposure, *C. albicans* 077 cells were washed twice with ice-cold 1X PBS and then incubated in 1 mL of a working solution of DCFH-DA at 37 °C for 30 min. The *C. albicans* 077 cells were treated with different concentrations of cfPNCs for 40 h, lysed in alkaline solution and centrifuged at 5000 rpm for 10 min. Then, 200 μL of the supernatant was transferred into the other fresh well of microtiter plate, and fluorescence was measured at an excitation of $A_{485\ nm}$ and emission of $A_{520\ nm}$ using a microplate reader (Bio-Rad laboratories Inc., Hercules, CA, USA).

3. Results and discussion

Developing biocompatible advanced functional materials with antimicrobial properties may be promising for environmentally benign applications. In this regard, polymer-based functionalized metal-oxide-based nanocomposite materials are of great interest due to their broad spectrum of antimicrobial potentials and applications in medicine. In this study, we have assessed the anticandidal activity of the polymer-functionalized $CoFe_2O_4$ NPs. Our results had shown that cfPNCs significantly kill *C. albicans* 077 cells at specific concentrations.

3.1. Synthesis and characterization of PANI/$CoFe_2O_4$ nanocomposite (cfPNCs)

The synthesis of cfPNCs was validated by the UV-visible spectrum recorded from A_{250} to $_{800\ nm}$ in NMP as a solvent. The typical UV-visible spectrum is shown in Fig. 1A; it showed two major distinctive peaks arisen through the presence of the PANI at positions ~$A_{330\ nm}$ and ~$A_{650\ nm}$. The absorption band around $A_{330\ nm}$ is attributed to the π–π^* transition of the benzenoid ring, and the peak around ~$A_{650\ nm}$ corresponds to the charge transfer from the benzenoid rings to the quinoid rings [37]. Besides that, the presence of the absorption peak at ~$A_{275\ nm}$ reflected the presence of $CoFe_2O_4$NPs embedded in the PANI matrix. The absorption peak at ~$A_{330\ nm}$ and ~$A_{650\ nm}$ corresponding to PANI were red and blue shifts in cfPNCs, respectively, owing to the presence of $CoFe_2O_4$ NPs (Fig. 1A). Thus, this result suggests that the interaction takes place between $CoFe_2O_4$ NPs and PANI chains. The absorption band widening towards the visible light region in case of cfPNCs was observed, and this has been used for the visible-light-driven ROS-mediated photocatalysis of various dyes [38]. The electronic structure of cfPNCs is characterized by the energy band gap, which is essentially the energy interval between the valence band (E_v) and the conduction band (E_c). The generation of a specific type of ROS such as $^{\bullet}OH$, $^1O_2$, or $O_2^{\bullet-}$ is governed by the metal-oxide-based NPs related to the energy band gap as well as by the redox potentials (E_H) of the different ROS generation reactions [33,39]. These ROS species induced by metal-oxide-based NPs have been established as the main mechanism of their antimicrobial action. Therefore, we have calculated the electronic band gap energy of cfPNCs from the absorbance data. The electronic band gap of the cfPNCs was determined by employing the Tauc relationship given below:

$$\alpha\ h\ \nu = A(h\ \nu - E_g)^n$$

whereas α is the absorption coefficient ($2.303A/t$), A is the absorbance and t is the thickness of the cuvette, B is a constant, h is Planck's constant, ν is the photon frequency, and E_g is the electronic band gap. The value of $n = 1/2, 3/2, 2$ or 3 depends on the nature of the electronic transition responsible for absorption and $n = 1/2$ for the direct band gap. An extrapolation of the linear region of a plot of $(\alpha h \nu)^2$ on the Y-axis versus the photon energy ($h\nu$) on the X-axis gives the value of the E_g, as shown in Fig. 1B. The E_g value of cfPNCs was determined to be 2.78, which shows it has good electron-transporting properties. Thus, cfPNCs can be used as an ROS-dependent anticandidal agent.

The XRD patterns of synthesized cfPNCs show well-resolved diffraction peaks, which can be assigned to the reflection planes (220), (311), (400), (422), (511), (440), and (844) of the $CoFe_2O_4$ NPs present in the PANI matrix (Fig. 1C). The reflection plane pattern was observed to be similar to the characteristics of the spinel cubic structure of $CoFe_2O_4$ {space group: *Fd*3 m (227), JCPDS card No. 22-1086} [40]. The mean crystalline size of $CoFe_2O_4$ NPs, calculated by the Debye–Scherrer equation, was found to

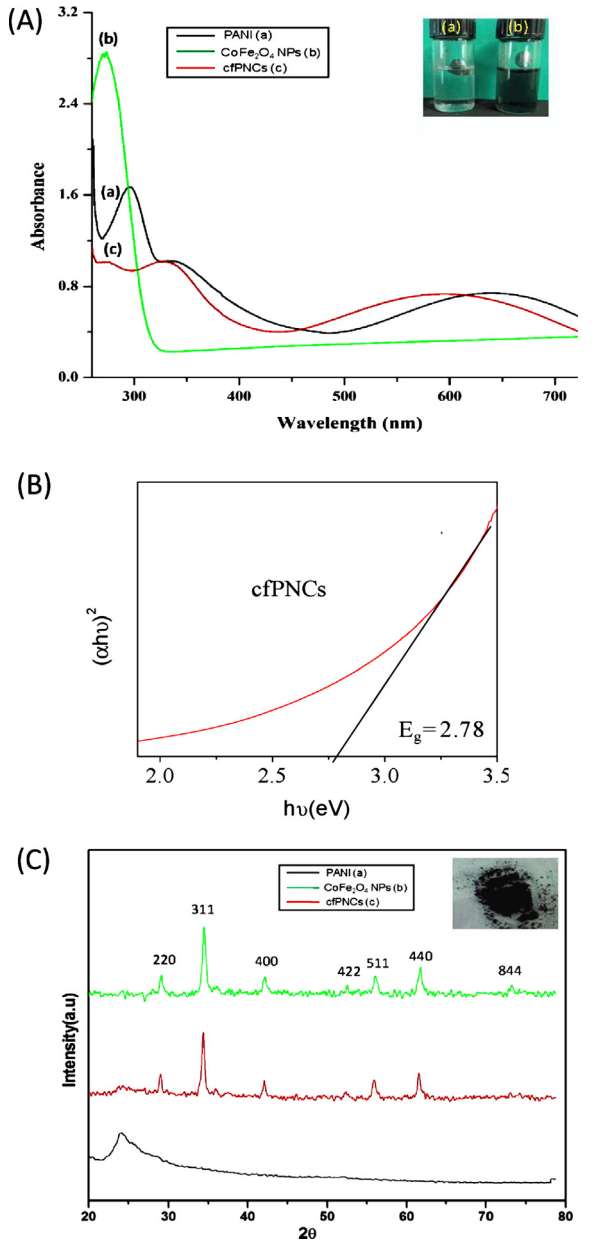

Fig. 1. (A) UV-visible absorption spectra of (a) PANI, (b) $CoFe_2O_4$ NPs and (c) cfPNCs were recorded between $A_{250\ nm}$ to $A_{800\ nm}$ using *N*-methyl-2-pyrrolidone (NMP) as a solvent. The inset in the figure depicts the NMP solution of as-synthesized (a) $CoFe_2O_4$ NPs and (b) cfPNCs, respectively. (B) Tauc plot depicting the energy band gap (E_g) of cfPNCs. (C) XRD patterns of (a) PANI, (b) $CoFe_2O_4$ NPs, and (c) cfPNCs, recorded in the 20°–80° 2θ angular range. (a) The peak at ~24.25° can be indexed as revealing the amorphous nature of PANI. (b) The XRD pattern of $CoFe_2O_4$ NPs evidenced well-resolved diffraction peaks, which can be assigned to reflection planes (220), (311), (400), (422), (511), (440), and (844). (c) As-synthesized cfPNCs XRD pattern, showing well-resolved diffraction peaks, which can be assigned to reflection planes (220), (311), (400), (422), (511), (440), and (844) of $CoFe_2O_4$ NPs embedded in amorphous PANI. The inset in the figure depicts the dried dark brown colour solid powder of synthesized CfPNCs.

be ~19.58. The additional peaks at ~24.25° depicted in Fig. 1C (a) can be indexed as reflecting the presence of amorphous PANI to the periodicity parallel and perpendicular to the polymer chains. The relative intensity of $CoFe_2O_4$ NPs diffraction peaks was reduced in cfPNCs compared with that of the bare $CoFe_2O_4$ NPs. Therefore, the results confirmed that the as-synthesized cfPNCs, PANI matrix encapsulated $CoFe_2O_4$ NPs.

The surface morphology and particle sizes of as-synthesized cfPNCs were determined by SEM, TEM, and AFM. The representative TEM micrograph of $CoFe_2O_4$ NPs is shown in Fig. 2A. The TEM micrographs shown in Fig. 2B exhibited a porous and well-interconnected irregular structure with irregular shapes and the porous nature of the cfPNCs is evidenced by TEM images taken at high magnification (Fig. 2C). The TEM micrographs indicate that the surface of cfPNCs was rough, with a more or less spherical morphology ranging from ~18 to 22 nm. The micrographs exhibited dark areas, indicating the presence of the $CoFe_2O_4$ NPs, while the bright area represents the PANI matrix encapsulated in the $CoFe_2O_4$ NPs (Fig. 2C). The microscopic results also confirmed that the PANI abridged the aggregation of $CoFe_2O_4$ NPs through repulsive forces between $CoFe_2O_4$ NPs and the PANI matrix. The agglomeration showed in the TEM images could be due to the preparation technique, as particle deposition on a copper grid and the drying process promote agglomeration [36].

The morphology of the cfPNCs powder was also examined by SEM, as shown in Fig. 2D. The results revealed the formation of micrometric aggregates consisting of nanometric spherical particles. Moreover, elemental analysis using EDAX (Fig. 2E) indicates the presence of Fe, Co, and O in as-synthesized cfPNCs. The atomic ratio of Fe to Co has to be found very close to the stoichiometric Fe/Co ratio in $CoFe_2O_4$ NPs, which further validates the existence of $CoFe_2O_4$ NPs entrenched in the PANI matrix. The AFM images also show the spherical morphology of cfPNCs in the size range between 12 and 21 nm (Fig. 3A and B), which is consistent with cfPNCs results obtained by TEM and SEM. The overall microscopic data confirmed that as-synthesized cfPNCs contain the nano-scale $CoFe_2O_4$ NPs with a more or less spherical shape.

The chemical structure of the as-synthesized cfPNCs was ascertained by FTIR spectroscopy. The FTIR spectra of the pure PANI and cfPNCs are shown in Fig. 4A. The spectrum of pure PANI revealed characteristic bands at positions 1580.54 cm^{-1}, 1498.32 cm^{-1}, 1303.12 cm^{-1}, 1148.44 cm^{-1}, and 818.93 cm^{-1}. The band positions at 1580.54 cm^{-1} and 1498.32 cm^{-1} were attributed to the characteristic C–C stretching of the quinoid and benzenoid rings, while the band position at 1303.12 cm^{-1} was assigned to the C–N stretching of the secondary aromatic amine. The bands at position 1148.44 cm^{-1} and 818.93 cm^{-1} reflect the aromatic C–H in-plane bending and the out-of-plane deformation of C–H in the 1,4-disubstituted benzene ring, respectively. The FTIR spectrum of cfPNCs exhibited the homology with pure PANI since, because of the higher mass of the participating atoms, vibrations of transition metal–oxygen bonds

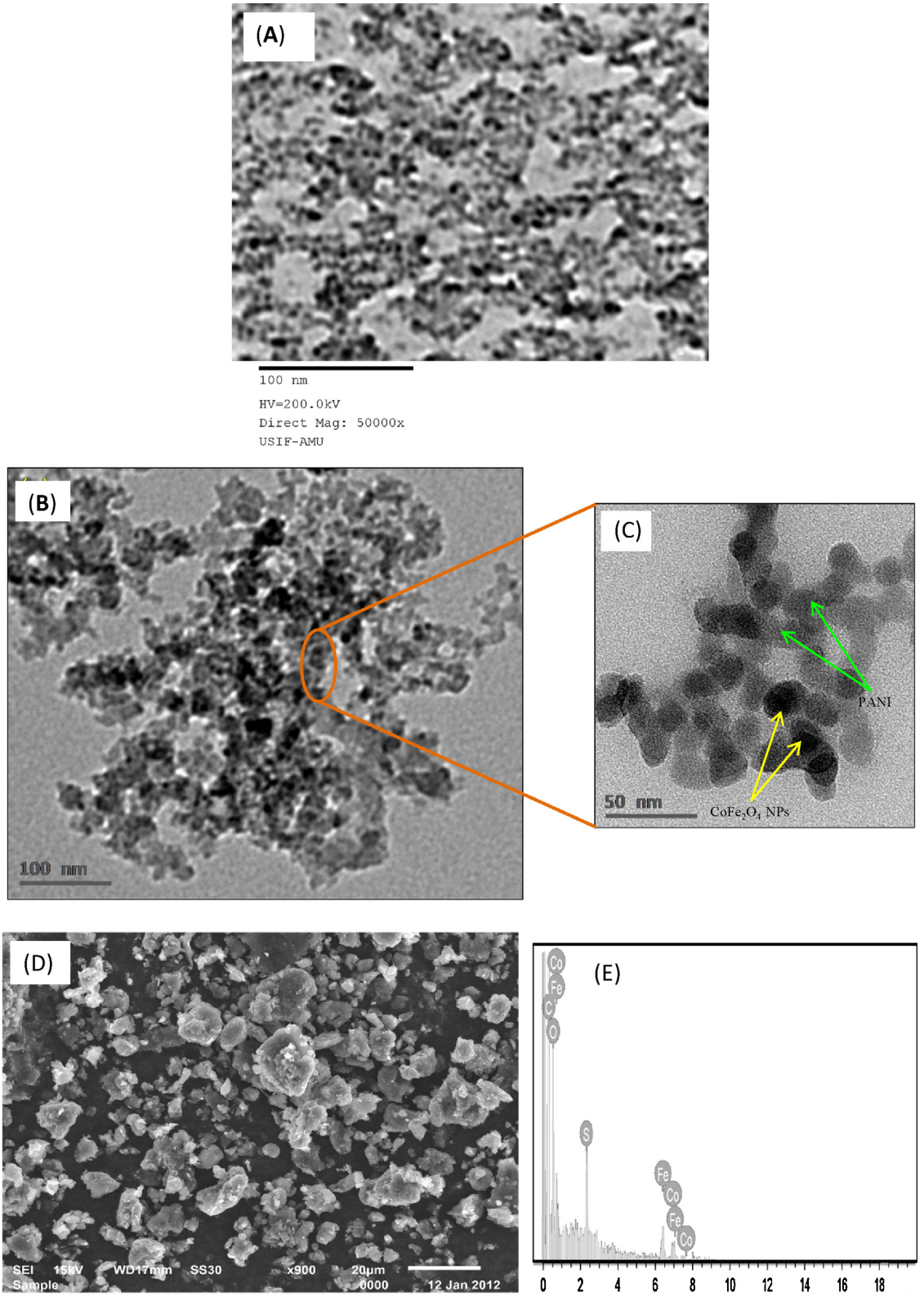

Fig. 2. (A) Transmission electron micrograph of $CoFe_2O_4$ NPs. (B and C) Transmission electron micrographs of cfPNCs exhibiting a porous and well-interconnected irregular structure with irregular shapes, at low and high magnifications, respectively. (D) Scanning electron micrograph of a cfPNCs powder, depicting micrometric aggregates consisting of nanometric spherical $CoFe_2O_4$ NPs in the PANI matrix. (E) EDAX spectrum, showing the elemental composition of cfPNCs and evidencing the presence of Fe, Co, and O.

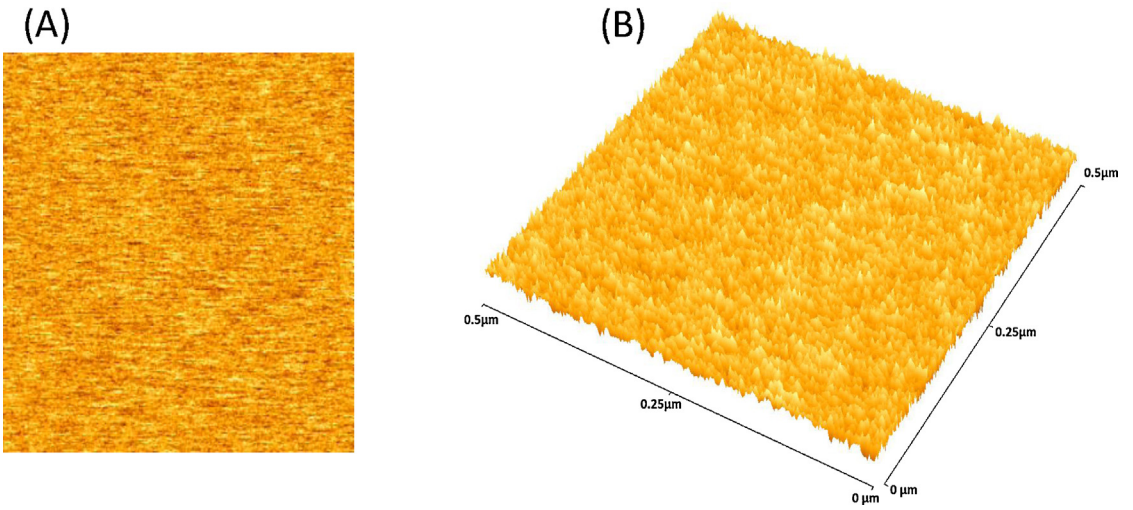

Fig. 3. Atomic force 2D (A) and (B) 3D micrographs illustrating the nanostructure of as-synthesized cfPNCs, respectively.

appear in the far-infrared region. These results indicate that there was some interaction between $CoFe_2O_4$ NPs and the PANI backbone. The FTIR spectrum of the cfPNCs exhibited that the deviations in the absorption bands at 1604.67 cm^{-1} and 1455.87 cm^{-1} can be assigned to the quinonoid ring and the benzenoid ring, respectively. It can be deduced that PANI in both pernigraniline form and emeraldine form are coexisting in the resultant composite. Furthermore, cfPNCs shows that the prominent stretching bands at 3440.54 cm^{-1} and 2923.12 cm^{-1} are assigned to the NH stretching vibrations for aromatic amine and –CH stretching, respectively. The change in the band's position clearly indicates that the NH group of the alanine ring interacts with the Fe^{2+} ions of the $CoFe_2O_4$ NPs. The presence of the additional band at position ~557.43 cm^{-1} is the signature band of Fe–O stretching; thus the data revealed the presence of $CoFe_2O_4$ in the PANI matrix [37].

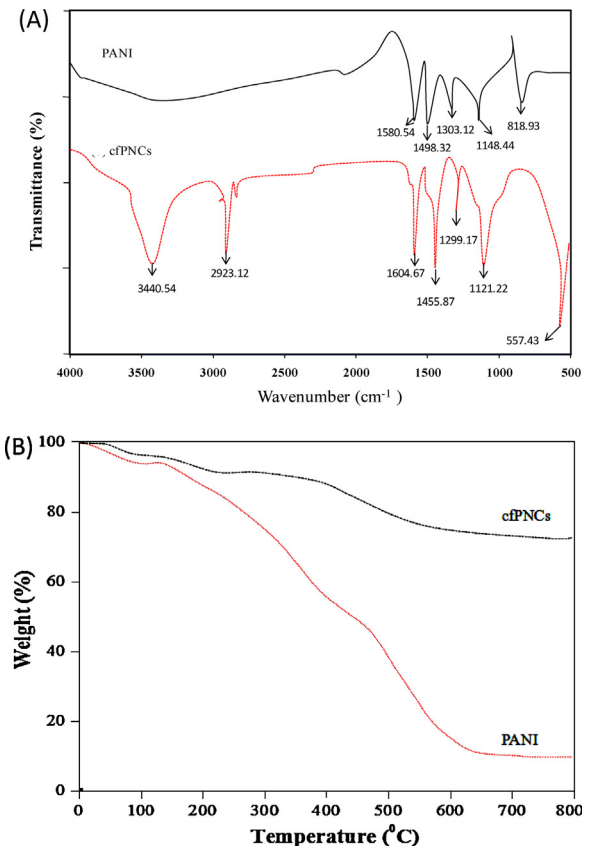

Fig. 4. (A) FTIR spectra, showing the interaction between the PANI and $CoFe_2O_4$ NPs in cfPNCs. (B) TGA graph, showing the thermal behaviour of PANI and cfPNCs.

The thermogravimetric analysis (TGA) analysis revealed the composition of cfPNCs (Fig. 4B). The TGA curve depicted the two weight loss steps of the pure PANI polymer; in the first step, it indicates a weight loss at a temperature up to ~110 °C, which may be ascribed to the eviction of a water molecule and of the dopant (HCl) from the PANI chains. The other weight loss step was observed in the ~200–600 °C temperature range, where the higher temperature causes volatilization and thermal degradation of the lower-weight PANI chains. TGA analysis of as-synthesized cfPNCs exhibited the highest thermal stability in contrast to the PANI. The TGA curve of the cfPNCs reveals a weight loss of ~22% at 500 °C. In contrast, pure PANI shows the same weight loss at 280 °C. The high thermal stability of cfPNCs is due to a strong interaction between PANI and $CoFe_2O_4$ NPs, which restricts the thermal motion of PANI in the composite. It also revealed that PANI itself was decomposed thermally within this temperature range, and that pure PANI has the great weight loss (~80%) at temperatures between 200 and 600 °C. The overall TGA data reveal that, in this study, the as-synthesized cfPNCs have the higher thermal stability, although the thermal stability of the cfPNCs depends on the amount of $CoFe_2O_4$ NPs that are present in the PANI matrix [34].

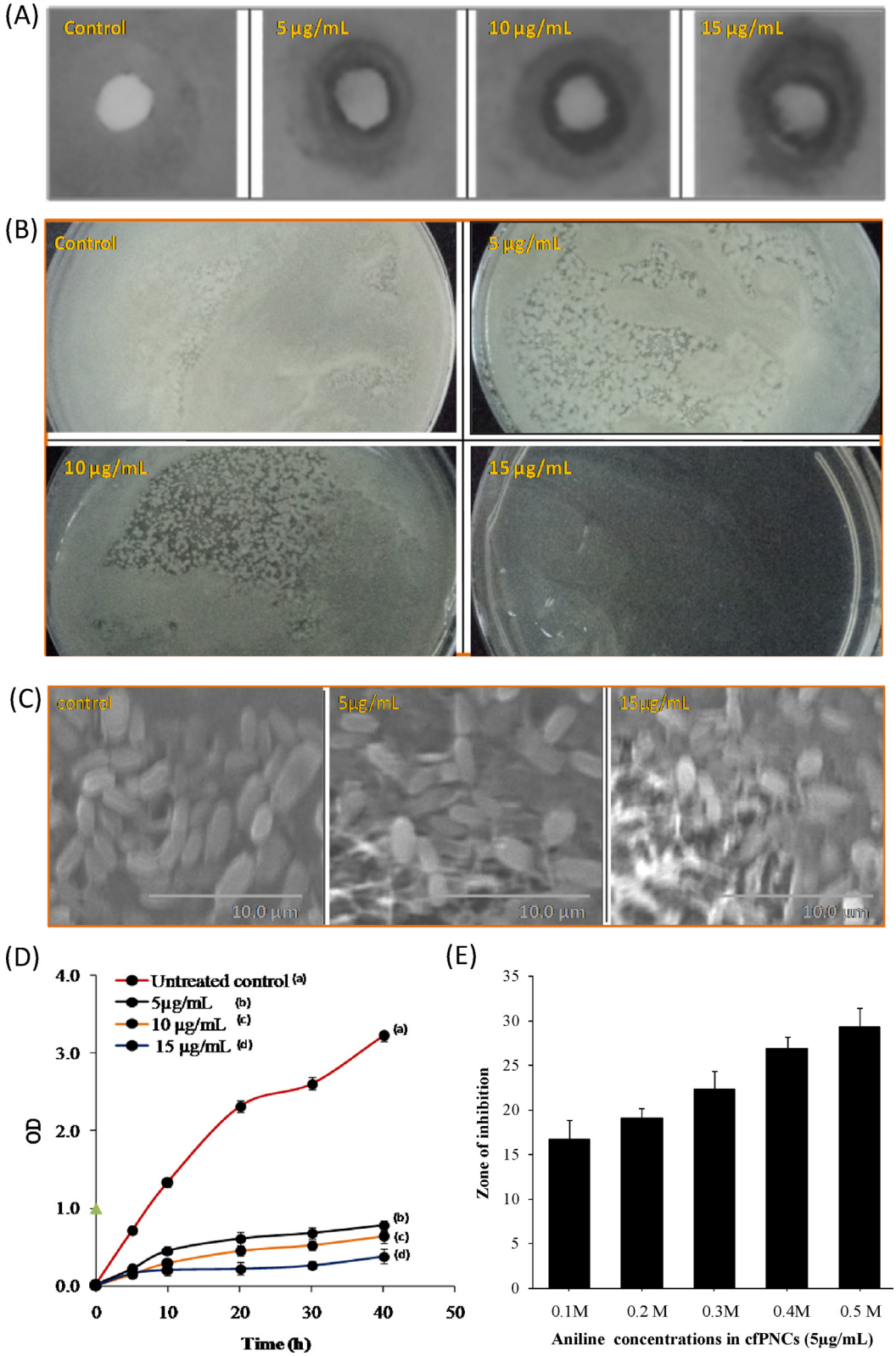

Fig. 5. (A) Inhibition zone and (B) *in vitro* killing assays showing the anticandidal activity of cfPNCs against *C. albicans* 077, respectively. (C) SEM-based observation of changes in the cell morphology of *C. albicans* 077 treated with cfPNCs (15 µg/mL). (D) Growth curve analysis giving the growth inhibition of *C. albicans* 077 in the presence of different concentrations of CfPNCs. (E) Effect of PANI on the antimicrobial activity of cfPNCs (5 µg/mL).

3.2. Anticandidal activity of PANI/$CoFe_2O_4$ nanocomposite (cfPNCs)

In light of the evidence of the rapid global spread of resistant clinical isolates of *C. albicans*, the need to find new anticandidal agents is of supreme importance. However, the past records of rapid, widespread emergence of resistance to newly introduced antifungal agents indicate that even new families of antimicrobial agents will have a short life assurance. Therefore, researchers are increasingly turning their attention to nanomaterials, looking for new leads to develop better nano-antimicrobial drugs against MDR *C. albicans* strains [41]. Therefore, in the current study, we have assessed the anticandidal activity of cfPNCs against MDR *C. albicans* 077. The disc diffusion and *in vitro* killing assays revealed that cfPNCs efficiently inhibits the growth of *C. albicans* 077 in a dose-dependent manner (Fig. 5A and B). Furthermore, SEM analysis of treated and untreated *C. albicans* 077 cells confirmed that cfPNCs have promising anticandidal activity (Fig. 5C). Growth-inhibition results based on the growth curve analysis of *C. albicans* in the presence of different concentrations of cfPNCs are shown in Fig. 5D. The untreated sample cells showed a normal pattern of growth with a lag phase of ~4 h, an active exponential phase of 8 to ~20 h before attaining the stationary phase. The anticandidal activity of cfPNCs leads to the significant concentration-dependent manner suppressed growth and delayed exponential phases of *C. albicans* 077 (Fig. 5D). The disc diffusion assay data revealed that the addition of different concentrations of PANI marginally enhanced the anticandidal activity of cfPNCs (Fig. 5E). PANI has inherent antimicrobial activity and shows growth inhibition of the bacteria and fungi under in vitro conditions [27,28].

The result shows that MDR *C. albicans* 077 was sensitive to cfPNCs with minimum inhibitory concentration (MIC) ~13.5 μg/mL of cfPNCs. The MIC is the lowest concentration of the compound at which the microorganism tested does not demonstrate visible growth. The almost complete cessation of growth was observed at a concentration of 15 μg/mL. However, a vast divergence {0.4–0.8 μg/mL silver NPs [42] to 2000 μg/mL selenium NPs [43]} in the MIC values of various kinds of NPs against *C. albicans* strains has been reported in the literature. These differences in the MIC values were probably attributed due to the strain type, the synthesis method, the NPs type, and their surface modifications, etc. The obtained anticandidal results of the current study corroborate our findings that have been published recently on the NP- and nanomaterial-mediated inhibition of the growth of *Candida* spp. [42,43].

3.3. Stability of PANI/$CoFe_2O_4$ nanocomposite (cfPNCs) in SD broth medium and during storage

We also determined the stability of cfPNCs (15 μg/mL) in a SD broth culture medium up to 72 h at 37 °C through the change in their UV-visible absorbance characteristics [33,36]. No significant change such as agglomeration and absorbance of cfPNCs has been noticed in the course of cell culture medium incubation (Fig. 6A), suggesting that the SD broth culture medium does not affect cfPNCs' stability,

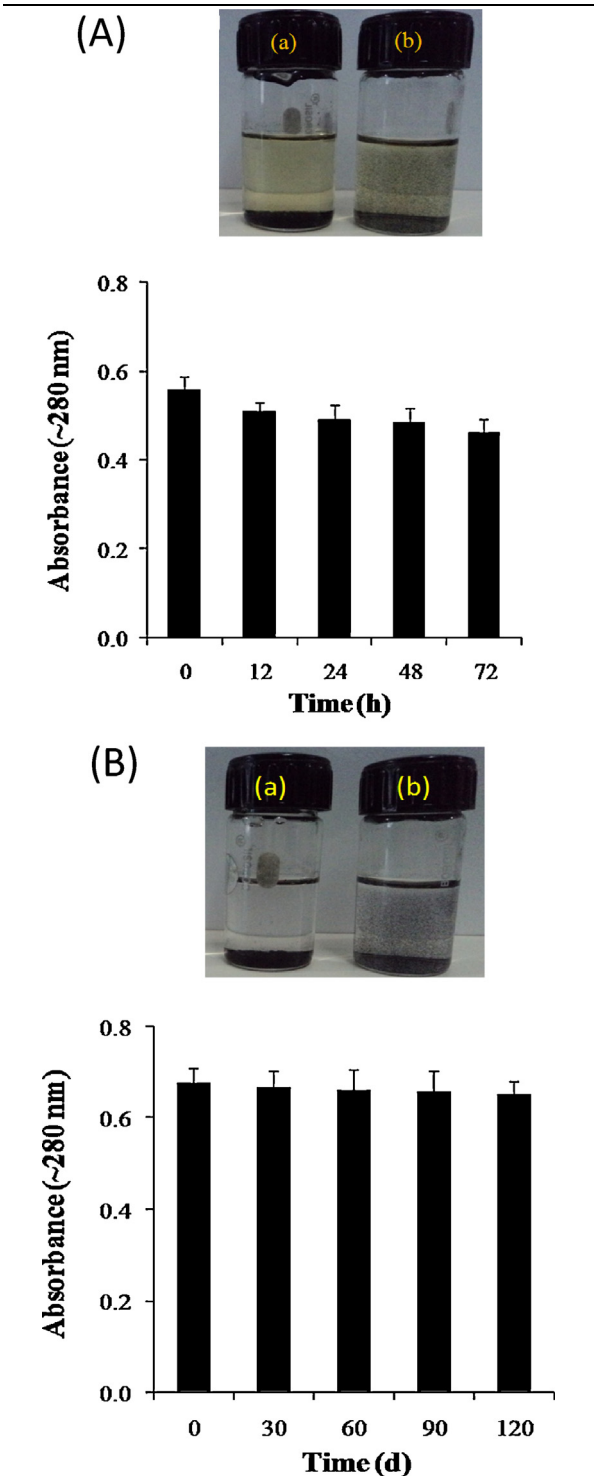

Fig. 6. (A) Stability of the (a) $CoFe_2O_4$ NPs and (b) cfPNCs in the SD broth medium. The stability of cfPNCs in the SD broth culture medium was monitored up to 72 h at 37 °C through the change in UV-visible absorbance characteristics. (B) Stability of the (a) $CoFe_2O_4$ NPs and (b) cfPNCs in an NMP solution during storage. The stability of cfPNCs in NMP was monitored up to 72 h at 37 °C through the changes in UV-visible absorbance characteristics. The bar graph illustrates the non-significant change in the absorbance of cfPNCs (15 μg/mL) after 120-day storage at 25 °C.

size and integrity. However, the incubation of the bare and surface modified NPs in the culture medium does not affect stability, size and integrity, respectively [36,44]. Also, it was observed that the colloidal solution of cfPNCs remained stable for 120 days and that there was no significant change in the absorbance (Fig. 6B).

3.4. Role of ROS produced by PANI/$CoFe_2O_4$ nanocomposite (cfPNCs) in anticandidal activity

In our recent study [33], ZnO NPs were shown to induce cell death of *C. albicans* 077 cells by ROS production. In light of these results, we cogitate that

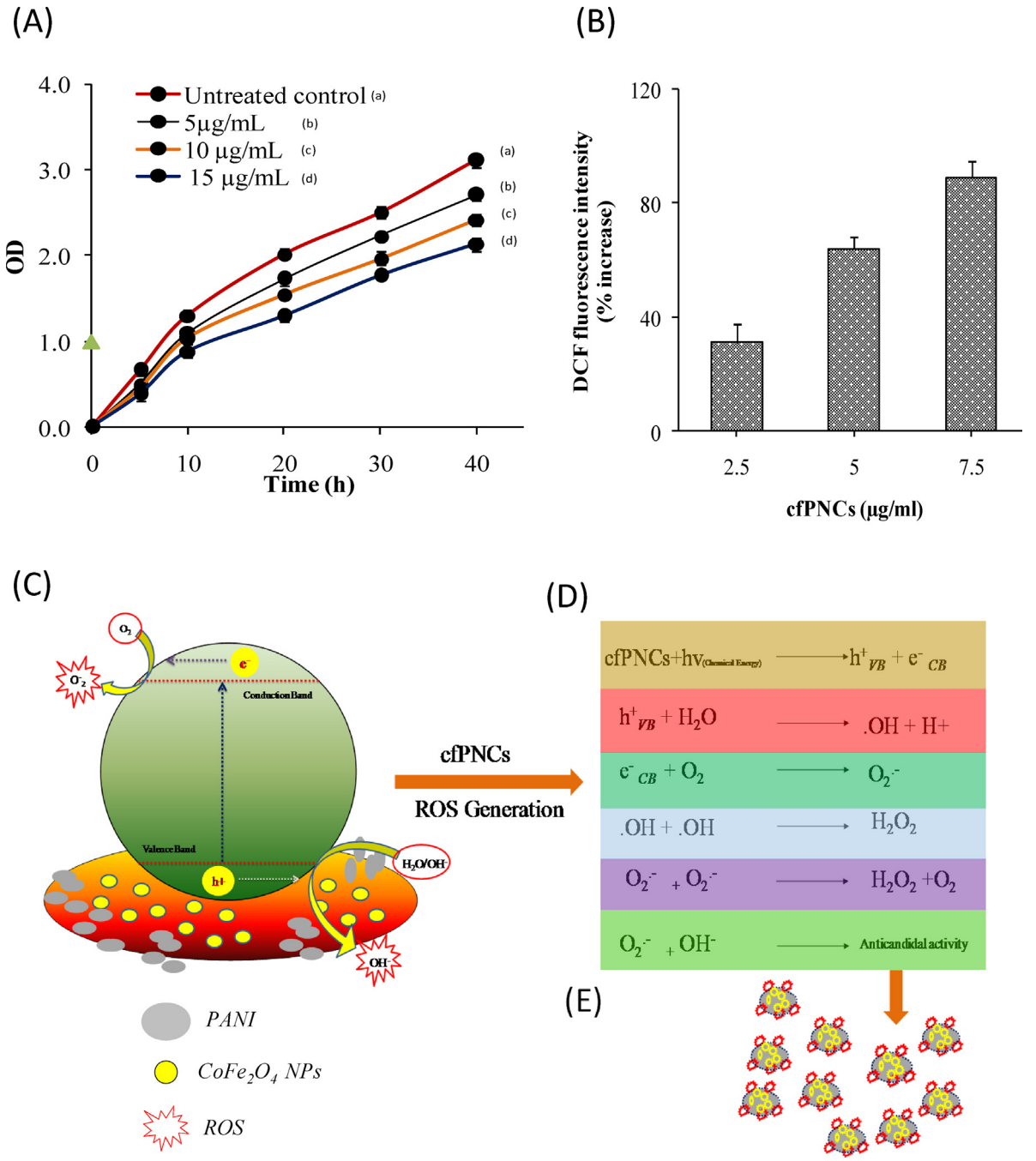

Fig. 7. Role of ROS produced by cfPNCs in anticandidal activity. (A) Analysis of the growth curve shows the protective effect of histidine (5 mM) on *C. albicans* 077 growth inhibition in the presence of different concentrations of cfPNCs. (B) Determination of the ROS production within the *C. albicans* 077 cells treated by different concentrations of cfPNCs. (C and D) Plausible mechanistic aspects of ROS generation by cfPNCs and their role in anticandidal activity. (E) cfPNCs inside the cytoplasm; they can interfere with energy production in mitochondria and promote the generation of ROS. ROS may cause cell-lysis and DNA damage in *C. albicans* 077.

the anticandidal effect of cfPNCs on *C. albicans* 077 may be mediated through ROS, even though oxidative stress induced by reactive oxygen species (ROS) is a well-known inducer of cytotoxicity and cell death in *C. albicans* [45]. We therefore tested whether the ROS produced by the cfPNCs are responsible for its inhibition of *C. albicans* 077 growth. The protective effect of histidine, a known scavenger of hydroxyl radicals and singlet oxygen, on the anticandidal activity of cfPNCs was tested by adding histidine (5 mM) to a *C. albicans* 077 culture containing cfPNCs at 15 μg/mL. Fig. 7A shows a protective effect of histidine on growth enhancement of *C. albicans* 077 in the presence of cfPNCs. Histidine (5 mM) almost completely protects *C. albicans* 077 from the anticandidal activity of cfPNCs. The fact that histidine reduced the effect of cfPNCs on *C. albicans* 077 viability (Fig. 7A) is supported by the ROS results shown in Fig. 7B, exhibiting a reduction in the amount of ROS produced within the *C. albicans* 077 cells treated with cfPNCs, after the addition of histidine. However, various researches have been done on the generation of ROS by various metal-oxide-based NPs. Recently, an electronic band gap structure of the metal oxides NPs with the redox potentials (E_H) has been correlated with different ROS generation reactions [14,19,39]. Thus, when cfPNCs gained a higher energy than E_g, the electrons (e^-) of $CoFe_2O_4$ NPs were promoted across the band gap to the conduction band (E_c), which creates a hole (h^+) in the valence band (E_c). These e^- in the E_C and holes in the E_v possibly have high reducing and oxidizing powers, respectively. The electrons react with molecular oxygen to produce the superoxide anion ($O_2^{\bullet -}$) through reductive reactions. The hole h^+ can abstract an e^- from water and/or hydroxyl ions to generate $^{\bullet}OH$ (Fig. 7C and D). The promising anticandidal activity demonstrated in this study was attributed to the enhancement of the rapid separation efficiency of e^- and h^+ through an electronic interaction between $CoFe_2O_4$ NPs and PANI [37,38]. Taken together, the results of this study confirmed that the ROS principally contribute to the anticandidal activity of the cfPNCs (Fig. 7E).

4. Conclusion

We have demonstrated here cfPNCs' anticandidal activity against *C. albicans* 077 by alleviating ROS-mediated oxidative stress and revealed possible underlying mechanisms. In future studies, we will suggest in-depth *in vitro* and *in vivo* studies that will help to identify cfPNCs' anticandidal potential for the management of diseases caused by MDR *C. albicans* isolates.

Acknowledgments

Financial support for this work through the Centre of Excellence in Materials Science (Nanomaterials), Department of Applied Physics, Z.H. College of Engineering & Technology, Aligarh Muslim University, Aligarh-202002, Uttar Pradesh, India is greatly acknowledged. B.R. Singh is greatly thankful to CSIR Govt. India for award of Pool Scientist.

References

[1] C. Yang, J. Du, Q. Peng, R. Qiao, W. Chen, C. Xu, Z. Shuai, M. Gao, J. Phys. Chem. B 113 (2009) 5052–5058.
[2] E.M. Geniès, A. Boyle, M. Lapkowski, C. Tsintavis, Synth. Met. 36 (1990) 139–182.
[3] A.J. Heeger, J. Phys. Chem. B 105 (2001) 8475–8491.
[4] I.H. Gul, A. Maqsood, J. Alloys Compds. 465 (2008) 227–231.
[5] H.M. Joshi, Y.P. Lin, M. Aslam, P.V. Prasad, E.A. Schultz-Sikma, R. Edelman, T. Meade, V.P. Dravid, J. Phys. Chem. C 113 (2009) 17761–17767.
[6] G.B. Alcantara, L.G. Paterno, F.J. Fonseca, M.A. Pereira-da-Silva, P.C. Morais, M.A.G. Soler, J. Nanofluids 2 (2013) 175–183.
[7] R. Prucek, J. Tuček, M. Kilianová, A. Panáček, L. Kvítek, J. Filip, M. Kolář, K. Tománková, R. Zbořil, Biomaterials 32 (2011) 4704–4713.
[8] D.W. Hwang, H.Y. Ko, J.H. Lee, H. Kang, S.H. Ryu, I.C. Song, D.S. Lee, S. Kim, J. Nucl. Med. 51 (2010) 98–105.
[9] L. Zhang, Y. Jiang, Y. Ding, M. Povey, D. York, J. Nanopart. Res. 9 (2007) 479–489.
[10] A. Azam, A.S. Ahmed, M. Oves, M.S. Khan, S.S. Habib, A. Memic, Int. J. Nanomed. 7 (2012) 6003–6009.
[11] J. Sawai, T. Yoshikawa, J. Appl. Microbiol. 96 (2004) 803–809.
[12] S. Arokiyaraj, M. Saravanan, N.K. Udaya Prakash, M. Valan Arasu, B. Vijayakumar, S. Vincent, Mater. Res. Bull. 48 (2013) 3323–3327.
[13] J. Hrenovic, J. Milenkovic, N. Daneu, R.M. Kepcija, N. Rajic, Chemosphere 88 (2012) 1103–1107.
[14] Y. Li, W. Zhang, J. Niu, Y. Chen, ACS Nano 6 (2012) 5164–5173.
[15] K.R. Raghupathi, R.T. Koodali, A.C. Manna, Langmuir 27 (2011) 4020–4028.
[16] M.J. Hajipour, K.M. Fromm, A. Akbar Ashkarran, D. Jimenez de Aberasturi, I.R.d. Larramendi, T. Rojo, V. Serpooshan, W.J. Parak, M. Mahmoudi, Trends Biotechnol. 30 (2012) 499–511.
[17] A.J. Huh, Y.J. Kwon, J. Controlled Release 156 (2011) 128–145.
[18] A. Carmona-Ribeiro, L. de Melo Carrasco, Int. J. Mol. Sci. 14 (2013) 9906–9946.
[19] H. Zhang, Z. Ji, T. Xia, H. Meng, C. Low-Kam, R. Liu, S. Pokhrel, S. Lin, X. Wang, Y.-P. Liao, M. Wang, L. Li, R. Rallo, R. Damoiseaux, D. Telesca, L. Mädler, Y. Cohen, J.I. Zink, A.E. Nel, ACS Nano 6 (2012) 4349–4368.
[20] S. Rana, J. Rawat, M.M. Sorensson, R.D.K. Misra, Acta Biomater. 2 (2006) 421–432.
[21] T. Gordon, B. Perlstein, O. Houbara, I. Felner, E. Banin, S. Margel, Colloids Surfaces A Physicochem. Eng. Aspects 374 (2011) 1–8.
[22] W. Zhou, L. Ding, J. Liu, Nano Res. 2 (2009) 593–598.
[23] N. Tran, T.J. Webster, J. Mater. Chem. 20 (2010) 8760–8767.
[24] B.S. Inbaraj, T.-Y. Tsai, B.-H. Chen, Sci. Technol. Adv. Mater. 13 (2012) 015002.
[25] R. Kumar, H. Münstedt, Polym. Int. 54 (2005) 1180–1186.
[26] H. Zuo, D. Wu, R. Fu, J. Appl. Polym. Sci. 125 (2012) 3537–3544.
[27] Z. Kucekova, V. Kasparkova, P. Humpolicek, P. Sevcikova, J. Stejskal, Chem. Pap. 67 (2013) 1103–1108.
[28] P. Boomi, H.G. Prabu, Colloids Surfaces A Physicochem. Eng. Aspects 429 (2013) 51–59.
[29] A. Gullo, Drugs 69 (Suppl. 1) (2009) 65–73.
[30] A. Lipovsky, Y. Nitzan, A. Gedanken, R. Lubart, Nanotechnology 22 (2011) 105101.
[31] G. Brambilla, F. Mattioli, L. Robbiano, A. Martelli, Mutagenesis 27 (2012) 387–413.
[32] R.M. Liang, Y.B. Cao, Y.J. Zhou, Y. Xu, P.H. Gao, B.D. Dai, F. Yang, H. Tang, Y.Y. Jiang, Acta Pharmacol. Sin. 31 (2010) 616–628.
[33] M. Shoeb, B.R. Singh, J.A. Khan, W. Khan, B.N. Singh, H.B. Singh, A.H. Naqvi, Adv. Nat. Sci. Nanosci. Nanotechnol. 4 (2013) 035015.
[34] G.D. Prasanna, H.S. Jayanna, A.R. Lamani, S. Dash, Synth. Met. 161 (2011) 2306–2311.
[35] J. Jiang, L. Li, M. Zhu, Reactive Funct. Polym. 68 (2008) 57–62.
[36] B.R. Singh, B.N. Singh, W. Khan, H.B. Singh, A.H. Naqvi, Biomaterials 33 (2012) 5753–5767.
[37] J.A. Khan, M. Qasim, B.R. Singh, S. Singh, M. Shoeb, W. Khan, D. Das, A.H. Naqvi, Spectrochim. Acta A Mol. Biomol. Spectrosc. 109 (2013) 313–321.
[38] P. Xiong, Q. Chen, M. He, X. Sun, X. Wang, J. Mater. Chem. 22 (2012) 17485–17493.
[39] C.D. Vecitis, K.R. Zodrow, S. Kang, M. Elimelech, ACS Nano 4 (2010) 5471–5479.

[40] Y. Wang, J. Park, B. Sun, H. Ahn, G. Wang, Chem.–Asian J. 7 (2012) 1940–1946.
[41] A.F. Wady, A.L. Machado, V. Zucolotto, C.A. Zamperini, E. Berni, C.E. Vergani, J. Appl. Microbiol. 112 (2012) 1163–1172.
[42] D.R. Monteiro, L.F. Gorup, S. Silva, M. Negri, E.R. de Camargo, R. Oliveira, D.B. Barbosa, M. Henriques, Biofouling 27 (2011) 711–719.
[43] Z.B. Kazempour, M.H. Yazdi, F. Rafii, A.R. Shahverdi, Ir. J. Microbiol. 5 (2013) 81–85.
[44] L. Wang, D. Nagesha, S. Selvarasah, M. Dokmeci, R. Carrier, J. Nanobiotechnol. 6 (2008) 1–15.
[45] Y. Zhou, G. Wang, Y. Li, Y. Liu, Y. Song, W. Zheng, N. Zhang, X. Hu, S. Yan, J. Jia, Antimicrob. Agents Chemother. 56 (2012) 3250–3260.